Version of Record: https://www.sciencedirect.com/science/article/pii/S0927024823004683
Manuscript_bece30e66129d029fb37867981e495de

Qualification of laser-weld interconnection of aluminum foil to back-contact silicon solar cells

Barry Hartweg[1,2], Kathryn Fisher[1,2], Jason Ro[1], Zachary Holman[1,2]
[1]Arizona State University, Tempe, AZ 85281
[2]SunFlex Solar, LLC, Tempe, AZ 85281

ABSTRACT

Laser welding can be used to interconnect high-efficiency back-contact silicon solar cells with low-cost Al foil. This interconnection approach is relatively new and, thus, requires detailed vetting of its reliability before being adopted commercially. In this study, we weld 50-µm-thick Al foil to Sunpower back-contact cells and observe that the laser-weld adhesion, module fill factor, and reliability through thermocycling are all highly correlated to each other. A JMP statistical model built from adhesion data reveals that the statistically significant parameters to improve laser-weld adhesion are the laser pulse energy, pulse density, and pattern. Increasing the laser pulse energy and density improves the foil adhesion to the cell metallization, which is likely because of the improved melting of the Sn capping layer on the Cu electrode of the cells, as identified by cross-sectional microscopy. 94.4% of the modules fabricated using laser welds with a mean adhesion above 0.8 mJ lost than 5% of their initial maximum power after 200 thermocycles, which is the IEC 61215 criterion for any single accelerated stress test. Additionally, 90.0% of modules fabricated with an as-fabricated module series resistance below 1.9 Ω.cm passed thermocycling. Thus, laser-weld adhesion and the as-fabricated module series resistance can be used in the further development of new laser-weld settings and as quality control parameters in the manufacturing of these modules.

INTRODUCTION

Back-contact (BC) cell structures have achieved some of the highest single-junction efficiency values for both silicon heterojunction and homojunction cells, reaching 26.7% and 26.1%, respectively [1-3]. Presently, there is no industry standard method for interconnecting BC cells—nearly every cell technology uses a different interconnection method. Traditional soldered ribbons are used for ZEBRA-BC cells, which are now in mass production. These cells are metallized with screen-printed Ag, and their modules use half-cut cells, achieving full-sized module efficiencies above 21% [4]. Sunpower BC cells are interconnected with a specially developed soldered tab that has built-in strain relief. These cells have Sn-capped Cu metallization, presumably deposited via electroplating. These modules have reached efficiencies up to 22.7% [5-8]. Another common interconnection method for commercial BC modules uses electrically conductive backsheets. This method typically uses a backsheet with a Cu foil on its inner surface (a "Cu backsheet") and conductive pastes to form the interconnection between the backsheet and cells. Cu backsheet interconnections have become commonplace for interconnecting metal wrap-through cell technologies, but this method has also been tested on ZEBRA BC cells [9-12].

The electrically conductive backsheet interconnection method adds notable materials cost to modules due to its use of Cu and conductive pastes, so there has been development to mitigate the use of these materials. For example, Bennett *et al*. tested an Al backsheet that still used conductive pastes to form a bond between the cells and the Al foil [13]. They found that a special coating and a deposited Cu film were needed on the surface of the Al backsheet prior to depositing Cu contacts and the conductive paste, in order to maintain low contact resistance throughout damp-heat testing. Additionally, work has been done to develop a laser-welding interconnection process that would mitigate the need for conductive pastes altogether. Schulte-Huxel *et al*. fabricated a BC mini-module with 25 x 125 mm^2 busbar-less strip cells that were metallized with 25-µm-thick evaporated Al; the cells were subsequently interconnected with a 10-µm-thick structured Al foil that was laser welded to the evaporated Al on the cells. This module architecture demonstrated less than 2% relative cell-to-module loss, which was

© 2023 published by Elsevier. This manuscript is made available under the Elsevier user license
https://www.elsevier.com/open-access/userlicense/1.0/

mostly due to short-circuit current losses from the laminate [14]. The same group also laser welded 10-µm-thick Al foil to the screen-printed Al paste on the rear of full-area Al-back-surface-field (Al-BSF) solar cells. This formed a durable interconnection that only experienced a 1.1% relative maximum power point (P_{MPP}) loss after 500 humidity-freeze cycles [15]. Paschen *et al.* used 8-µm-thick Al foil to interconnect busbar-less shingled solar cells by forming laser welds at the screen-printed Al and Ag fingers and on the passivated regions (for additional mechanical robustness) [16]; 3 out of 5 of their laser-welded shingled mini-modules experienced less than a 5% relative P_{MPP} loss after 200 thermocycles (TC). These examples of laser-welded interconnections utilized thin (8–10 µm) Al foil. The shingled-cell modules did not exhibit a notable fill factor (*FF*) loss from lateral transport in these thin foils because of the low short-circuit currents of the strip cells [14, 16]. In the case of the laser-welded full-area Al BSF cells, the Al foil covered the full area of the rear side of the wafer, where the lateral resistance through the tin foil was compensated by its large width [15]. If such thin Al foil were applied to a full-wafer-sized BC cell, it would lead to undesirable *FF* losses, as the Al must be patterned to reach each contact each polarity. This patterning reduces the width of foil through which the current may travel, and thus the foil must be thicker instead. We previously demonstrated robust laser-weld interconnection between 45-µm-thick Al foil and the screen-printed Ag busbars of full-wafer-sized ZEBRA-BC cells. These modules exhibited a *FF* loss less than 2% relative after 200 TC [17]. However, the laser welds were made with a millisecond laser that does not easily scale to the throughputs of manufactured solar modules.

As laser welding has yet to be implemented in commercial silicon solar modules, this interconnection method requires detailed vetting of its reliability before deployment. Perhaps the most important IEC 61215 accelerated degradation test for stressing a new interconnection is the TC test [18]. This test applies a thermomechanical stress by varying the temperature from −40 °C to 85 °C at a rate of 1 °C per minute with 10-minute dwell times at the temperature extremes and current applied to the modules during the heating steps [19]. We have observed that poorly adhered foil interconnects experience dramatic failures in TC; for example, Al-foil-interconnected BC mini-modules that did not have any welds lost more than 20% of their intial P_{MPP} after 200 TC [17]. We thus submit that excellent performance in TC testing is required of these modules before any additional reliability testing or upscaling should be performed.

This work demonstrates a robust nanosecond laser-welding process that interconnects Cu-metallized BC cells with Al foil. A wide range of laser parameters are explored to find settings that produce measurable adhesion without damaging the solar cell. Peel tests are performed for a variety of laser-weld settings, and the results are correlated to module performance in TC to determine the mechanical requirements needed from the laser welds to withstand TC testing.

EXPERIMENTAL DETAILS

The mini-modules in this study were fabricated at ASU using one Sunpower E60 BC cell per module; these cells are readily available from online suppliers. The fabrication process required a two-step lamination, where the rear Al foil is left exposed for laser welding after the first lamination; a schematic of the module stack at the time of welding is provided in Figure 1. The first lamination step was performed at a low temperature of 95 °C for 3 minutes. At this point, the module consisted of tempered glass, ethylene vinyl acetate (EVA), the BC cell, a 50-µm-thick middle-patterned insulator (MPI), and two coplanar 50-µm-thick sheets of Al foil (one for each polarity and each

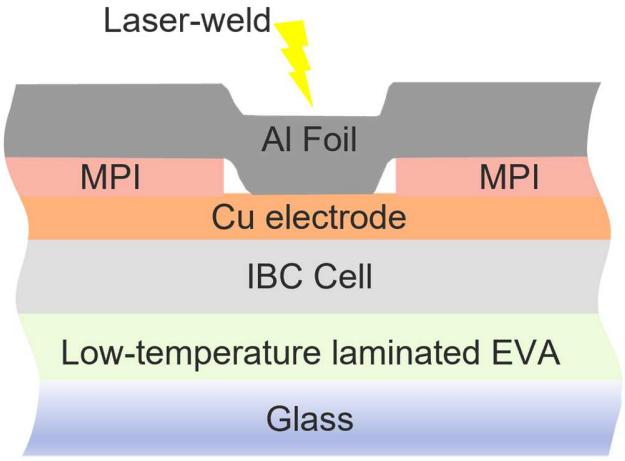

Figure 1. Schematic of the mini-module or peel test sample stack at the time of laser-welding. Mini-modules were laminated at 95 °C and peel samples were laminated at 110 °C.

about one-third the size of the cell, so that they do not touch each other in the middle of the cell). The MPI is an electrically insulating polymer sheet with adhesive of each of its faces. It was laser cut using a CO_2 laser to remove six 3.5 x 1.5 mm^2 rectangles aligned with the intended solder points of the cell; these openings allow three points of contact per polarity between the Al foil and the metal electrodes of the BC cell. After the 95 °C lamination, the Al foil was hand-embossed through the openings in the MPI to ensure the Al foil makes physical contact with the electrodes of the BC cell. Laser welding was then performed with a 1064 nm YLPN Series pulsed ytterbium fiber nanosecond laser from IPG Photonics. Top-down microscope images of the laser-weld patterns that were used in this study are presented in Figure 2. (Note that, throughout this paper, each of the patterns seen in Figure 2 is referred to as one weld, although the laser makes hundreds or thousands of pulses per such weld pattern.) Most laser patterns used two welds per MPI opening (*e.g.* spiral and star patterns); the only exception is that of the 6 x 7 grid of lines, where only one was used per MPI opening. These patterns were tested with a variety of laser settings that are specified below. After welding all six MPI openings and laying-up a rear EVA layer and a transparent polymer backsheet, the modules were laminated at 145 °C for 18 minutes. Prior to placement in the TC chamber, modules were electrically characterized via Suns-V_{OC} and current-voltage (*I-V*) measurements. Suns-V_{OC} and *I-V* testing were performed on a Sinton Instruments FMT-500 flash tester. The mini-modules were then loaded into an environmental chamber and ran for 200 TC. After the TC testing, the modules were remeasured to observe any losses in P_{MPP}. The TC process varied the chamber temperature from -40 °C to 85 °C at a rate of 1 °C per minute with 10 minute dwell times. However, there was no current applied to the modules, so this process slightly deviated from the true IEC 61215 standard [19].

Peel test samples were fabricated similarly to mini-modules, with a few exceptions. Cells were cut into ~20 mm wide strips that retained the solder/weld points but removed the grid of fingers in the middle of the cells. The glass used was untempered and cut to accommodate the smaller cell strip size. The MPI openings were 8 x 16 mm^2 rectangles to allow ample room for the laser weld to unravel during the peel process. The low temperature, 3-minute lamination occurred at 110 °C, allowing for better adhesion and fixturing of the MPI to the cell than a lamination at 95 °C. The peel samples were hand embossed prior to laser welding in the same manner that modules were. It is worth noting that we assume that the physical contact between the foil and cell contacts after hand embossing is comparable in the peel samples as they are in the modules, despite the different sizes in the MPI openings. The Al foil is quite ductile and appears conformal upon visual inspection, so this appears to be a reasonable assumption. After welding, 5-mm strips are laser cut in the foil, which is used to perform the peel test. The peel strip is narrower than the opening in the MPI, so there was no adhesion contribution from the MPI during the peel measurement of the weld. There was no second lamination at 145 °C, leaving the Al foil exposed. The peel tests were performed on a Jinlong 90° peel tester, running at 100 mm/min, and the resulting peel force was measured using an Imada DS2-

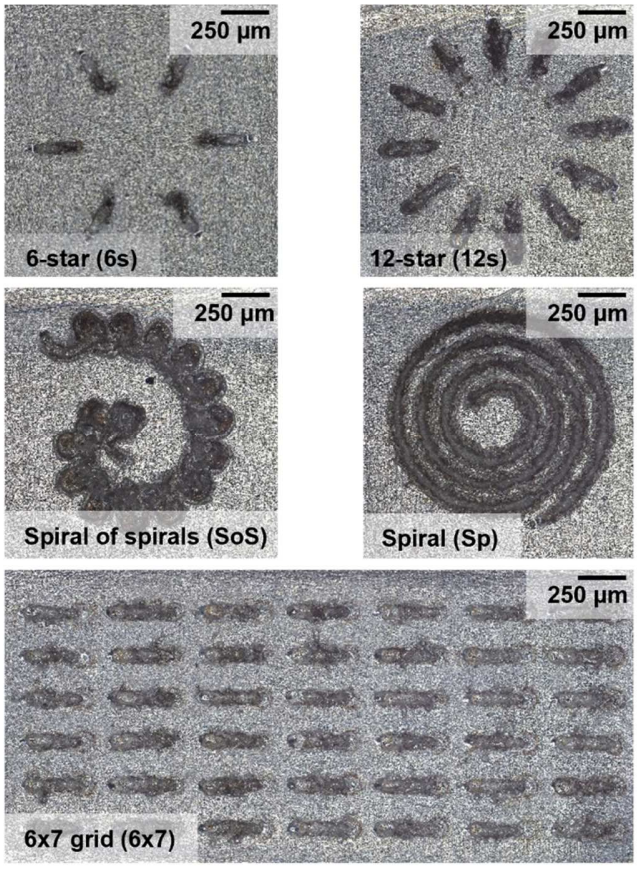

Figure 2. Top-down microscope images of the different laser patterns used throughout this study. These images were taken "as-welded" with the Al foil still in place.

11 force gauge. The peel values reported in this study represent the energy required to peel the laser welds at 90° for a single MPI opening. The values were calculated by integrating the curve for each laser weld on the peel force vs. distance plot, giving units of N.mm or mJ. Integrating the peel curves allows for direct comparison of peel values and incorporates differences in weld shape and area.

Welds were examined with visible-light microscopy using a Keyence VHX-7000 confocal microscope. This allowed images to appear in focus across the sample regardless of the topography of the sample, and it provided a simple method to estimate the penetration depth of laser welds. A Zeiss Auriga scanning electron microscope (SEM) with energy-dispersive X-ray spectroscopy (EDS) capabilities was also used to image and collect elemental maps of laser weld cross-sections. Mini-modules used for cross-section analysis were fabricated using a semi-rigid polymer frontsheet instead of glass; the metal and Si layers were then cut with the IPG laser and the polymer layers were cut with the CO_2 laser. Samples were mounted in epoxy and mechanically ground and polished to expose a cross-section of the weld with the Al foil layer intact. Rear EVA and backsheet were not applied to samples used for microscopy.

RESULTS AND DISCUSSIONS

Screening for appropriate laser-weld settings

When testing laser settings in initial screens, we observed that there are three broad categories of laser-welds: under-welded, appropriately welded, and over-welded. Examples of each are presented in Figure 3. These samples were prepared like peel-test samples and imaged after peeling off the Al foil in order to show the effect of the laser weld on the surface of the cell's electrode. The under-welded case is shown in Figure 3a; in this example, only a fraction of the laser pattern actually interacted with the surface of the cell, suggesting that the laser settings did not provide enough energy to penetrate the full thickness of the Al foil across the entire laser pattern. These types of laser welds exhibit adhesive failure with minimal or no adhesion due to the minimal penetration of the weld into the cell electrode. Thus, they are unacceptable from a mechanical and reliability standpoint.

In the over-welded example in Figure 3c, there is an oval-shaped region near the bottom of the image—outlined on the middle weld line—that has penetrated through to the front of the Si cell. In a detailed study on the recombination caused by laser welding Al foil on different passivated surfaces, John *et al*. showed that some laser settings resulted in as little as an 18 fA/cm^2 increase in a recombination current density after welding, but other settings caused an increase of nearly 1000 fA/cm^2 [20]. Although some penetration of the passivation layers may be tolerated by some

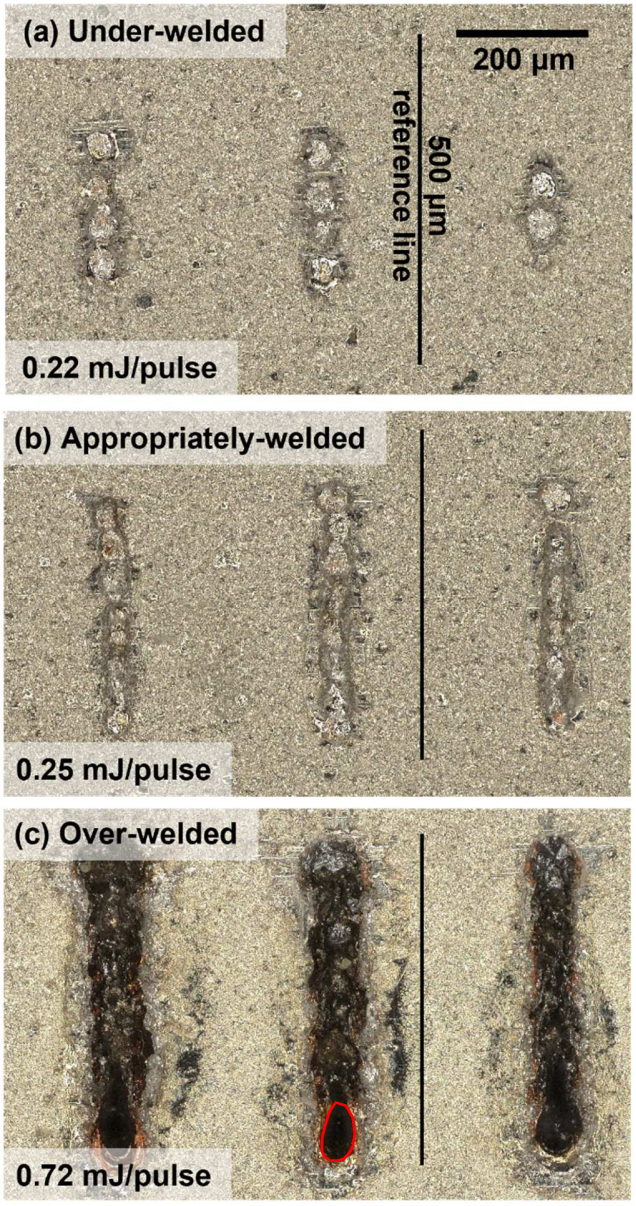

Figure 3. Confocal microscope images of the surface of the cell electrode after laser welding and Al foil removal. Three different welds were prepared using the same pulse density (500 pulses/mm) and pattern (three 0.5 mm lines). Only the pulse energy was varied.

cell technologies, this is not our experience with these Cu-metallized BC cells. In our studies, if enough energy was provided by the laser to penetrate the 50 µm of Al and 30 µm of bulk Cu, it was also able to penetrate the entire 150 µm of Si in the cell. Thus, settings like those that resulted in Figure 3c are not useful due to the problematic shunting and passivation damage that would be caused by these welds, regardless of their adhesion.

Figure 3b shows an acceptable laser-weld setting, where the laser pattern has fully transferred to the cell's electrode but has only interacted with the electrode and did not damage the Si. These settings also produce nonzero adhesion of the Al foil to the cell. Peel tests most commonly exhibit a failure of the Al foil material itself with a small amount of cohesive failure around the edges of the laser pattern. After peeling the Al foil, Al material is left behind in the laser-welded area and often the Al foil that was removed has a cut-out that resembles the laser-welded pattern. There is a range of pulse energy values between that of Figure 3b and 3c that are likely to produce acceptable welds.

Important laser parameters to promote adhesion

Within the "appropriately-welded" category, there are several laser parameters that can be controlled to fine-tune the laser interaction with the cell's electrode, including pulse duration, frequency, patterning speed, welded area, and the pattern traced by the laser. However, it is not initially obvious which are the most important to promote adhesion. Thus, we designed a series of experiments to test a range of laser settings and patterns on peel samples, and to use the resulting data to build a model that can predict the role of these parameters on adhesion. The least-squares fitting method was utilized in the JMP statistical software package [21]. A number of JMP models were tested using different combinations of factors that pertained to the laser and weld pattern settings. The model selected for discussion in this study achieved the highest F ratio (lowest signal-to-noise ratio) and predicted that most of the factors in the model to be statistically significant. Note that factors were considered statistically significant with a p-value below 0.05 in the two-tailed t-test (Prob > |t|). The peel data, the predicted values, and the predicted equation from the JMP model are shown in Figure 4. The predicted equation itself is listed at the bottom of Table 1.

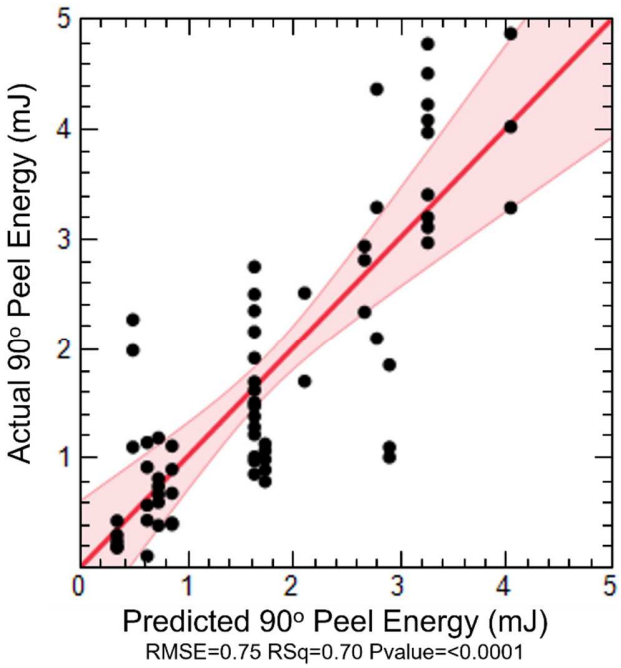

Figure 4. The black points represent the measured peel energy values and the values predicted from a linear JMP model with three factors: pulse energy, pulse density, and laser pattern. The red line is the predicted equation, and the red shaded region represents the 95% confidence interval around the mean values.

Table 1. Parameter estimate table for each factor used in the JMP model for predicting peel energy of laser welds. The predicted equation from the JMP model is listed below the table.

Factor	Coefficient estimate	Std Error	t Ratio	Prob>|t|
$E_{pulse,}$ Pulse energy (mJ)	11.1	2.0	5.41	<.0001
$d_{pulse,}$ Pulse density (mm^{-1})	$6.46x10^{-3}$ N.mm^2	$1.1x10^{-3}$	6.00	<.0001
$P_{laser,}$ Laser Pattern[6 star]	-2.06 mJ	0.32	-6.40	<.0001
$P_{laser,}$ Laser Pattern[12 star]	-1.95 mJ	0.31	-6.30	<.0001
$P_{laser,}$ Laser Pattern[6x7]	-0.577 mJ	0.41	-1.41	0.164
$P_{laser,}$ Laser Pattern[SoS]	1.49 mJ	0.32	4.65	<.0001
$P_{laser,}$ Laser Pattern[Spiral]	2.76 mJ	0.29	9.61	<.0001

Predicted Equation

$$E_{peel} = P_{laser} + 11.1E_{pulse} + (6.46x10^{-3}\,N.mm^2)d_{pulse} - 5.52\ mJ$$

The selected model included the following factors in a linear formula: pulse energy, pulse density, and laser pattern. The pulse energy value is the integral of the pulse power over time curve, the pulse density is the pulse frequency multiplied by the laser-patterning speed, and the laser pattern is one of those shown in Figure 2. All three of these factors were statistically

Table 2. Summary of the laser-weld settings and pattern combinations used in this study.

Unique Identifier	Graph symbol/color	Laser Pattern	Pulse energy (mJ)	Pulse Density (mm^{-1})	Energy density (mJ/mm)	Welded area (mm^2)	90° Peel Energy ± std. dev. (mJ)	Peel test sample size
6s-1	★	6-star	0.333	700	233	0.45	0.63 ± 0.41	5
12s-1	✱	12-star	0.333	700	233	0.90	0.73 ± 0.27	6
12s-2	✳	12-star	0.333	1000	333	0.90	2.04 ± 0.46	3
SoS-3	⊗	Spiral of spirals	0.163	400	65.0	1.10	0.26 ± 0.09	6
SoS-4	⊗	Spiral of spirals	0.163	480	65.0	1.10	0.69 ± 0.31	5
SoS-5	⊗	Spiral of spirals	0.163	600	97.5	1.10	1.45 ± 0.39	15
SoS-6	⊗	Spiral of spirals	0.333	500	167	1.10	3.24 ± 1.14	3
6x7-1	□	6x7 grid	0.333	700	231	1.58	2.10 ± 0.57	2
6x7-2	□	6x7 grid	0.333	1000	333	1.58	4.05 ± 0.79	3
Sp-5	○	Spiral	0.163	600	96.7	2.03	1.55 ± 0.55	9
Sp-6	○	Spiral	0.333	500	167	2.03	0.97 ± 0.14	5
Sp-7	○	Spiral	0.254	500	127	2.03	2.30 ± 0.44	10

significant according to the p-values from the two-tailed t-test ($p < 0.0001$), as shown in Table 1. The only exception was the coefficient given for the 6 x 7 grid laser pattern, which had a p-value of 0.164. This high value is most likely due to an insufficient sample size, or an insufficient number of settings tested with this pattern. The R^2 of the predicted equation was relatively low at 0.70, which is mostly attributed to the large weld-to-weld variation in adhesion. Thus, this predicted equation may not be able to reliability predict the exact adhesion of a weld, but it does suffice to explain the general trends.

The pulse energy and density trends from this JMP model are similar to what Schulte-Huxel *et al.* observed, where the tear-off stress of Al-coated-glass laser welded to evaporated Al on a Si wafer increased as a function of laser pulse energy and the number of overlapping pulses [22]. In our JMP model, the magnitudes of the laser pattern coefficients can be directly compared to each other, demonstrating which laser patterns are more likely to produce well-adhered welds for a given set of laser settings. For example, the model predicts that both "star" patterns are likely to have worse adhesion than the spiral-type patterns with the same laser settings. One might expect that the adhesion should increase as a function of the welded area, but this underestimates the complexity of the relationships. In an alternate JMP model (not presented), welded area was considered as a factor instead of laser pattern but did not come out to be statistically significant, which led to a less convincing model than the one provided in Figure 4 and Table 1. This is likely because welded area alone does not account for the self-heating effects that occur in, for example, the spiral-type patterns.

Spiral of spiral (SoS) laser-pattern case study

The JMP model elucidates the dependencies of weld adhesion on laser settings, and thus served as a guide in selecting 12 settings—listed in Table 2, with their associated peel energies—to use in making mini-modules. Additionally, a unique symbol is given for each laser pattern, and a color is assigned to represent the specific combination of laser settings. These colored symbols are used in the figures hereafter. The listed welded area is a calculated parameter, assuming a 0.1 mm width across the programmed pattern geometry.

A study was conducted to isolate the effects of laser pulse density and pulse energy without varying the laser-weld pattern. Peel test samples and mini-modules were fabricated using four settings with the same SoS pattern

(see settings SoS-3 to SoS-6 in Table 2). The adhesion values and their resulting mini-module *FF* values are plotted in Figure 5. Pulse energy and pulse density were multiplied to give a "laser energy density" quantity in units of mJ/mm in order to make comparisons across the two different pulse energies studied. Dashed blue lines denote the range of *FF* (Figure 5a) and series resistance (R_s) (Figure 5b) values across two soldered mini-module references.

As Figure 5c reveals, the adhesion values increase linearly with laser energy density; note that the first three points (SoS-3-5) used the same pulse energy values and only varied in their pulse densities, while SoS-6 used a higher pulse energy than the first three points. This increase in adhesion corresponds to an decrease in mini-module R_s, but, above approximately 1.5 mJ peel energy, the cell's R_s itself becomes the major limiter of the mini-module R_s instead of the laser weld's contact resistance. As seen in Figure 3c, it is possible for the laser to damage the Si bulk, which would lower the pseudo-*FF* (*pFF*) and open-circuit voltage (V_{oc}). Fortunately, even in the most extreme setting, SoS-6, the *pFF* and V_{oc} were comparable to those of the other mini-modules, indicating that no damage was caused by laser welding.

Figure 6 displays a microscopy study on samples made with the laser settings from Figure 5 to better understand the underlying physical differences responsible for the adhesion and *FF* differences. The study included both top-down microscopy, before and after peeling the Al foil, as well cross sections to visualize interactions between the Al foil and the Cu electrode. Figure 6a is a low-magnification image of the SoS-3 cross section to show the entirety of the weld that is captured within the cross section; the estimated location of this feature is marked in Figure 6b by a red line. It is important to note that, in a cross-sectional view, only a single "slice" of the weld is visible, so it can be difficult to draw conclusions about the entirety of the weld from a single image. Thus, it is helpful to directly examine cross sections of samples with multiple laser settings to better draw conclusions about the relative trends that arise. Figure 6b provides a grid of microscopy images to compare all four of the SoS welds from a variety of perspectives. Note that the

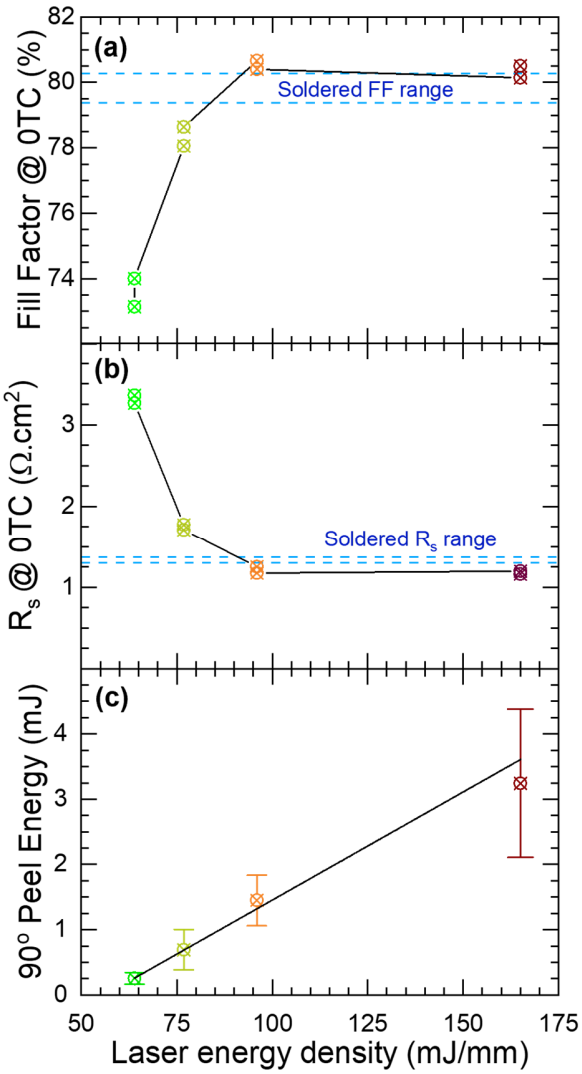

Figure 5. (a) Mini-module *FF*, (b) mini-module R_s, and (c) the peel energy of sister samples as a function of laser energy density, which is the product of the laser pulse energy and density from Table 2. All samples were made with the SoS laser pattern. The black line in (a) is a guide to the eye and the blue dashed lines represent the range of two soldered reference mini-modules. The black line in (b) is a linear regression of the mean values, and the error bars represent the standard deviations of

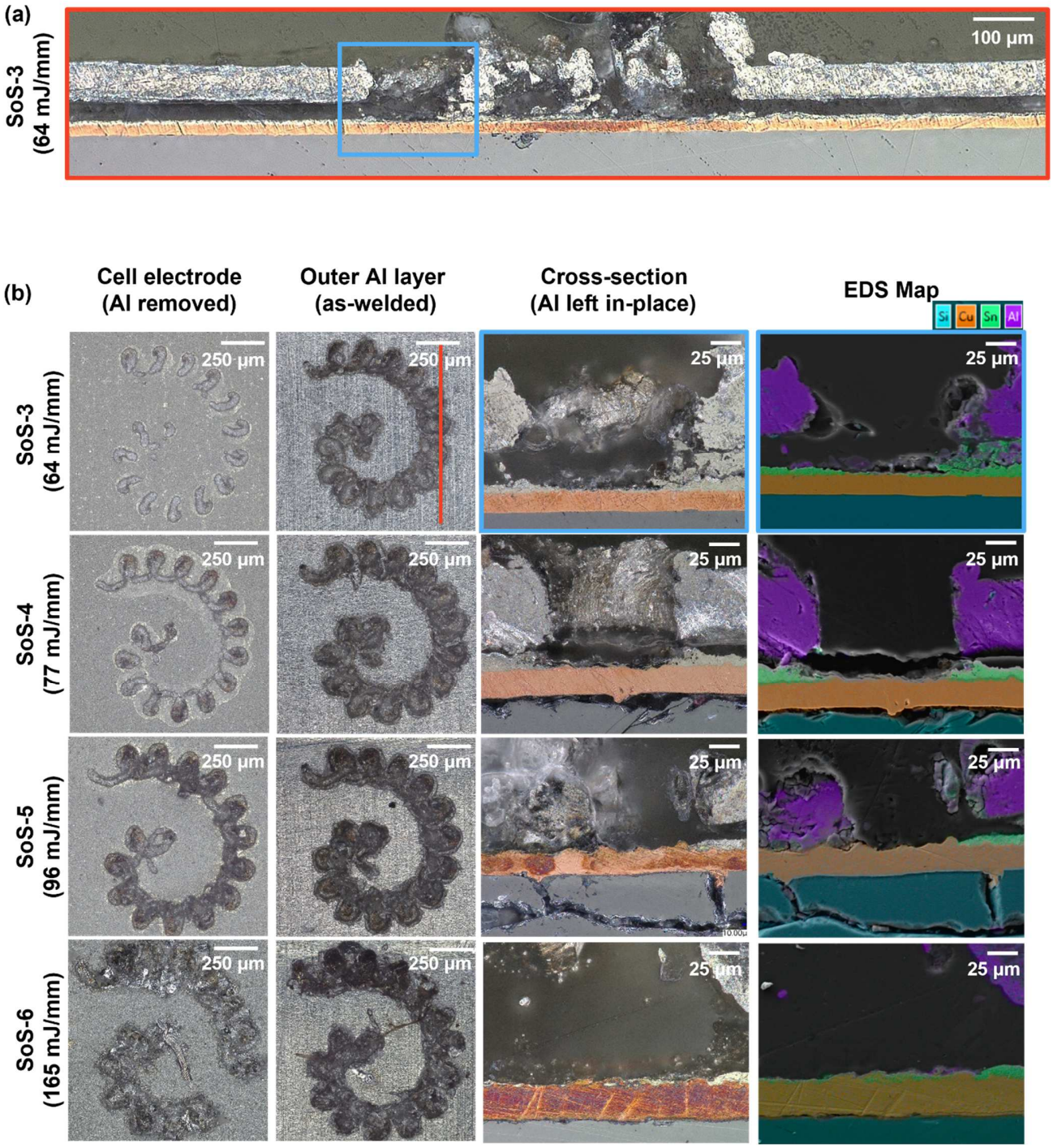

Figure 6. (a) Low-magnification microscope image of the SoS-3 cross-section. The red line marked on the "Outer Al layer" image of SoS-3 shows an estimate of where this cross-sectional "slice" is on the sample (b) *Cell electrode*: Top-down microscope images after the Al foil is peeled off, following laser welding, to expose the cell electrode. *Outer Al layer*: Top-down microscope images after laser welding, with the Al left in place. *Cross-section*: SEM images of the samples from the "Outer Al Layer" column after potting in epoxy and polishing. Cracks and defects in the Si are a result of the cleaving of the cell in sample preparation. *EDS map*: Elemental maps of the images from the "Cross-section" column. The legend in the top right indicates the elemental color code used.

“Outer Al layer (as-welded)” and “Cross-section” images are of the same samples before and after cross-section preparation, respectively. Meanwhile the “Cell electrode (Al removed)” images were recorded on separate peel samples. Recall from the experimental details, cross-section samples did not receive the second lamination step; thus, they were left without a rear EVA layer and rear backsheet. Portions of the welded area were laser-cut out of the cell, potted in epoxy, grinded, and polished down to expose the laser-welded region. The polymer material that appears above the Al foil is the epoxy from the potting process—not EVA. Bear in mind, also, that this sample preparation process is highly prone to the creation of artifacts such as cracks in the Si wafer, specks of material outside of their expected regions, disconnected Al foil, among others.

The effect of the laser weld on the surface of the cell’s electrode can be understood from the first column of Figure 6b. With the SoS-3 setting, the laser pattern did not fully transfer to the surface of the electrode; the pattern transferred primarily in the regions of the pattern that overlapped with each other (*i.e.,* the laser passed over the same area more than once). In the case of the SoS-4 and SoS-5 settings, there is some orange discoloration in this overlapped region, suggesting that the Sn capping layer has been penetrated, exposing the copper underneath. This is further validated when looking at the cross-sections and EDS maps: There remains a thin layer of Sn in the middle of the SoS-3 weld, while this layer is largely removed in the SoS-4, 5, and 6 welds. The Sn appears to pool around the walls of the weld in SoS-3. In the SoS-3 weld, there is also some intermixing of the Al and Sn clearly observed, while there are only faint Sn signals coming from the Al regions in the SoS-4, 5, and 6 welds, which may be attributed to material transfer during the polishing process. The individual elemental maps can be found in the supplemental figure S1.

Across all four of the laser-weld settings in Figure 6, there are portions of the Al foil that are missing. We attribute this to the ablation of the Al foil that is caused by the laser-welding process. It is worth noting that there is some deformation of the Cu material (seen most notably in SoS-4 and 5). However, it is unclear from these data alone whether this is an effect caused by the laser-welding process or if it is an artifact caused by the grinding and polishing involved with the sample preparation. There is deformation of Cu on the wafer side that is conformal to the cracks in the Si, which leads us to believe that it may be an artifact caused by polishing.

Even after studying the cross-sections in Figure 6, it is difficult to say precisely what is responsible for the adhesion observed in Figure 5, but the Sn layer appears to be an indicator. Our primary hypothesis is that the melting and redistribution of the Sn layer is largely responsible for both the mechanical and electrical performance of these laser-welds. The SoS-3 weld, which gave the worst adhesion out of all welds in Table 2, is the only weld in the SoS subset that still had Sn remaining even at the deepest point of laser penetration. In the other three SoS welds, there are regions where the Sn is missing from the Cu surface. The Sn melt pool area may increase with increasing laser energy density, and, if the Sn is responsible for bonding to the Al foil, the larger melt pools would enhance adhesion. A larger area of melted Sn would also increase the electrical contact area, which would decrease contact resistance between the cell electrode and the Al foil, explaining the decrease in R_s that was observed with increasing adhesion in Figure 5.

Expanding to other laser patterns

In Figure 7, the initial R_s of each mini-module fabricated with the laser settings listed in Table 2 is plotted against the respective mean peel energy value of its sister peel sample. Also included are reference *FF* and R_s ranges of the two reference soldered mini-modules and the average ± standard deviation values from four Al-foil-interconnected mini-modules without welding. (Note that it is often possible to measure *I-V* curves on unwelded modules due to the pressure contact formed by the lamination process, but the modules are highly inconsistent and unreliable). The *FF* and R_s trends that were observed in Figure 5 for the SoS laser patterns are largely repeated across the other laser patterns as well. In this dataset, 13 out of the 16 modules that used a laser setting that produced welds with an average peel energy of 0.8 mJ or higher (denoted by the vertical gray dashed line) had R_s values as good as or better than that achieved by soldering. One of the 6x7-1 mini-modules had a notably higher R_s than the other. We mostly attribute this to some misalignment that was observed. The 6x7 laser-weld patterns are quite large relative to the size of the MPI openings and the outer portions of the laser pattern were mistakenly patterned over the MPI area instead of on the cell's electrode. Thus, the weld adhesion seen within the mini-module itself is likely lower than what was measured on the sister peel samples, which had larger MPI openings. It is worthwhile to note that not all modules with R_s values lower than the soldered references modules had better or equivlanet FF to the soldered reference modules—and vice versa. This highlights the importance of using R_s to narrow-in on the electrical and mechanical bond formed by the the laser-welds without convoluting it with shunt resistance effects.

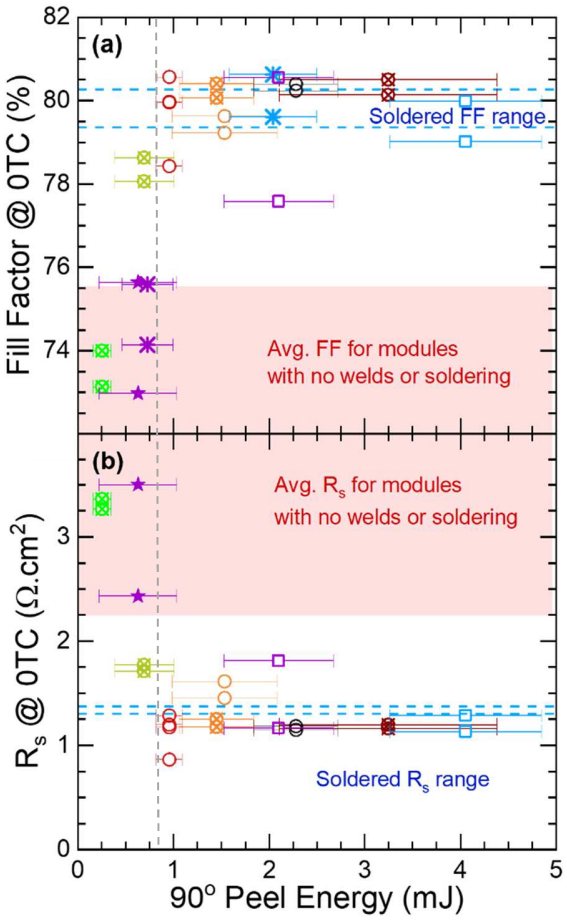

Figure 7. Avg. ± std. dev. peel energy values plotted against their corresponding mini-module (a) *FF* and (b) R_s values as-fabricated before any TC stress testing. The blue dashed lines represent the range of two soldered reference mini-modules, and the red shaded region represents the avg. ± std. dev. values from four Al foil interconnected mini-modules without any laser welds. Refer to Table 2 for the laser-weld legend.

It is interesting to compare and contrast the findings from Figure 7 with the results by Paschen *et al.* They reported similar *FF* values (>79%) with weld peak peel force values less than 0.1 N, compared to peak peel force values of about 0.9 N for our SoS-5 settings. Their Al foil interconnection, however, used hundreds (or perhaps thousands) of laser welds that were distributed across the entire rear-side of the cell [23]. Meanwhile, our modules are welded only in a substatially smaller area—the six MPI openings, which total a theoretical maximum contact fraction of 13%. Thus, this technology requires better mechanical and electrical bonding to achieve a sufficiently low contact resistance to accommodate all of the cell's current flowing through these six points of contact.

Laser welds through thermocycle testing

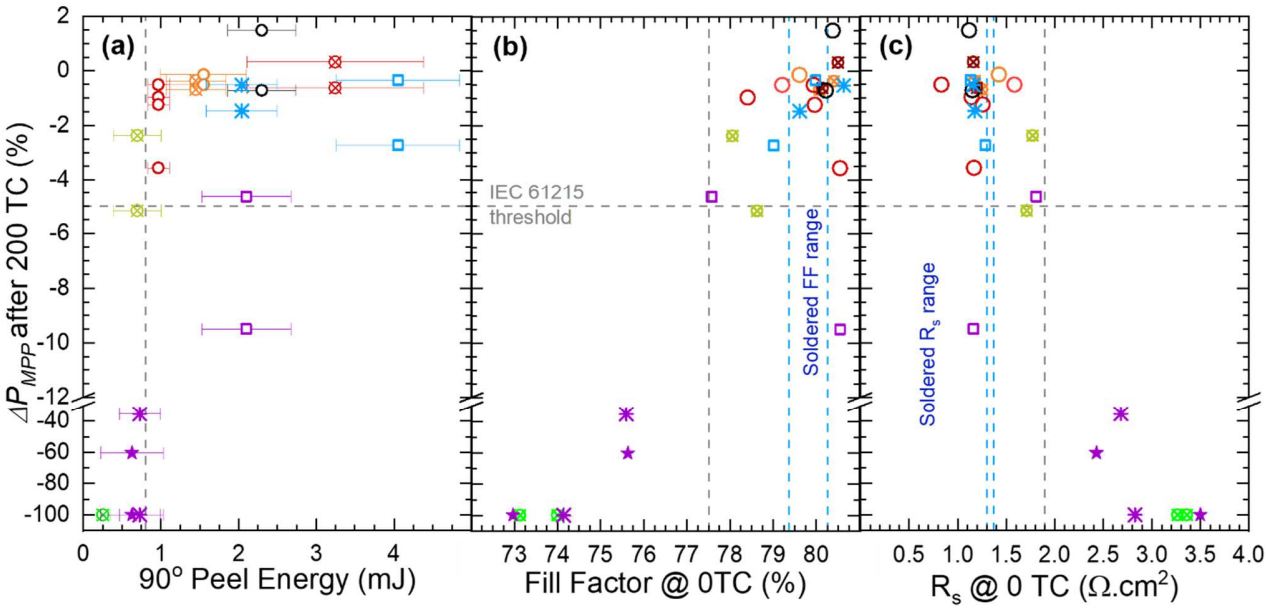

Figure 8. Relative change in P_{MPP} after 200 TC of mini-modules plotted against (a) laser-weld peel energy and (b) mini-module initial FF. The blue dashed lines represent the range of two soldered reference mini-modules. Refer to Table 2 for the laser-weld legend. A horizontal reference line is included at the -5% mark to indicate the threshold for passing IEC 61215. The vertical reference lines are proposed cutoff values for identifying laser-weld settings and fabricated modules that warrant further testing.

To understand the durability of mini-modules made with the laser settings in Table 2—and how that durability is correlated with laser weld and initial module quality—we plot the relative change in their P_{MPP} after 200 TC in Figure 8 against their peel values and their initial *FF* values before TC testing. Note that the threshold to pass the IEC 61215 TC test is a decrease of less than 5% of the original P_{MPP} after 200 cycles; a reference line is included on the plots to denote this cutoff [19]. Figure 8a includes a reference line for a peel energy of 0.8 mJ, and Figure 8b-c include similar lines for an initial *FF* of 77.5% and an initial R_s of 1.9 Ω.cm^2. These represent our estimates of the minimum values needed to have high confidence that the module will pass TC. The values were selected to incorporate the highest percentage of modules that lost less than 5% of their P_{MPP} through 200 TC. In the case of the 0.8 mJ reference line, 17 of 18 modules that had laser-weld adhesion higher than this passed TC, while only 1 in 8 modules with adhesion lower than this passed. The reference lines for both *FF* and R_s incorporate the same modules. 18 of 20 modules with an initial R_s lower than 1.9 Ω.cm^2 or with an initial *FF* higher than 77.5% passed TC *FF,* while all 6 modules with initial R_s and *FF* values outside of these specifications failed. While in this dataset the initial R_s and *FF* were well-correlated, this may not always be the case. We submit that initial R_s is a better metric to understand the quality of the interconnection without convoluting it with shunt resistance effects that would be captured with *FF*. Thus, we will exclude the reference *FF* from the remainder of this discussion.

One of the modules that was an outlier—and exception to these guidelines—was fabricated with the 6x7-1 laser-weld settings. This had a peel energy greater than 0.8 mJ and an initial R_s lower than 1.90 Ω.cm but still failed TC. Recall that the 6x7 settings gave lower-than-expected initial *FF* values in Figure 7. Oddly, the 6x7-1 module that failed TC was the module with the *lowest* initial R_s (1.22 Ω.cm^2) out of the four modules made with the 6x7 laser pattern, whereas the module with the *highest* initial R_s (1.89 Ω.cm^2) and laser-weld misalignment survived TC. We do not presently understand the underlying cause, but we suspect that this laser pattern may be considerably less consistent than the other patterns tested, and that the variations observed in this small sample set would not be statistically significant within a much larger set of both peel samples and mini-modules made with this laser pattern.

Note that many of the laser-weld settings with the lowest adhesion values failed catastrophically, with P_{MPP} losses between 35% and 100%. These failures are even worse than what we observed previously with un-welded ZEBRA-IBC modules, which experienced a 20% loss in P_{MPP} after 200 TC. The ZEBRA-IBC mini-modules utilized embossed Al-foil busbars that covered the entire surface of the wafer, whereas the Al foil only contacts the Sunpower cell electrodes at the 6 discrete MPI openings on the outer edges of the cell. Thus, the ZEBRA-IBC mini-modules have a greater contact area between the Al foil and cell electrodes than the Sunpower mini-modules, minimizing the likelihood of the Al foil becoming completely disconnected, *i.e.,* 100% P_{MPP} loss [17].

From Figure 8, there are five laser-weld settings that yielded modules with initial R_s values that were comparable to or lower than that achieved with soldering, and that subsequently passed TC. These are the 12s-2, SoS-5, SoS-6, 6x7-2, and Sp-7 settings, which, interestingly, used four different laser patterns and four different laser pulse energy and density combinations, suggesting that it is likely possible to achieve adequate laser welds across a wide variety of laser patterns if the appropriate corresponding laser parameters are used. These reference values can guide the development of future laser-weld settings: Laser welds with adhesion below 0.8 mJ are likely not worth testing in an actual module, and modules with initial R_s values above 1.90 $\Omega.cm^2$ are likely not worth testing in TC. This is extremely useful to know in order to expedite the development of new laser-weld settings. Of course, the R_s reference value is convoluted with cell-level R_s effects; thus, ideally the cell R_s would be measured prior to module fabrication to know that it is within an expected cell R_s range.

CONCLUSIONS

The laser pulse energy, density, and pattern were found to be statistically significant parameters for the adhesion between the Al foil and the BC cell electrode. Cross-sectional microscopy revealed that higher adhesion and R_s seems to be related to the amount of the Sn coating on the Cu electrode of the BC cell that melts and is redistributed during welding. The laser-weld adhesion and module initial R_s were found to be highly correlated to module performance in TC testing. Of the 18 modules fabricated with laser welds that had a mean peel energy of 0.8 mJ or higher, 17 of these—or 94.4%—passed TC testing, losing less than 5% relative of their initial P_{MPP}. Of the 20 modules fabricated with laser welds with an initial R_s of 1.90 $\Omega.cm^2$ or higher, 18 of these—or 90.0%—passed TC. Thus, this adhesion reference value could be used as a guideline in the development of laser welds prior to applying them to modules, and this initial R_s reference value could be used as a simple quality control metric in a production line to pass or reject modules. While this work focused on TC testing, which we have observed to accelerate a prominent failure mechanism in improperly welded modules, subsequent studies should stress the interconnections with additional relevant tests such as current-loading through TC, humidity-freeze, and mechanical loading.

ACKNOWLEDGEMENTS

The information, data, or work presented herein is also funded in part by the U.S. Department of Energy, Office of Energy Efficiency and Renewable Energy, under Award Number DE-EE0007538.

REFERENCES

[1] M. A. Green *et al.*, "Solar cell efficiency tables (Version 60)," *Progress in Photovoltaics: Research and Applications,* https://doi.org/10.1002/pip.3595 vol. 30, no. 7, pp. 687-701, 2022/07/01 2022, doi: https://doi.org/10.1002/pip.3595.

[2] K. Yoshikawa *et al.*, "Silicon heterojunction solar cell with interdigitated back contacts for a photoconversion efficiency over 26%," *Nature Energy,* vol. 2, no. 5, p. 17032, 2017/03/20 2017, doi: 10.1038/nenergy.2017.32.

[3] F. Haase *et al.*, "Laser contact openings for local poly-Si-metal contacts enabling 26.1%-efficient POLO-IBC solar cells," *Solar Energy Materials and Solar Cells,* vol. 186, pp. 184-193, 2018/11/01/ 2018, doi: https://doi.org/10.1016/j.solmat.2018.06.020.

[4] R. Kopecek *et al.*, "ZEBRA technology: low cost bifacial IBC solar cells in mass production with efficiency exceeding 23.5%," in *2020 47th IEEE Photovoltaic Specialists Conference (PVSC)*, 15 June-21 Aug. 2020 2020, pp. 1008-1012, doi: 10.1109/PVSC45281.2020.9300503.

[5] S. H. Gerritsen, "Reverse engineering the SunPower generation III solar cell," Eindhoven University of Technology, 2018.

[6] M. Sickmoeller, "IBC Technology & Manufacturing," ed. Maxeon Solar Technologies, 2020.

[7] "SunPower Maxeon Solar Panels." Maxeon Solar Technologies, Ltd. https://sunpower.maxeon.com/int/solar-panel-products/maxeon-solar-panels (accessed.

[8] "Maxeon Gen II Solar Cells." SunPower. https://us.sunpower.com/sites/default/files/sp-gen2-solar-cell-ds-en-a4-160-506760e_0.pdf (accessed.

[9] P. C. De Jong, "Achievements and challenges in crystalline silicon back-contact module technology," Netherlands, 2010-03-15 2010.

[10] Bennett and N. Loiseaux, "Measurement of Strains in MWT Modules During Manufacture," *Energy Procedia,* vol. 27, pp. 697-702, 2012/01/01/ 2012, doi: https://doi.org/10.1016/j.egypro.2012.07.132.

[11] G. Beaucarne *et al.*, "Study of Compatibility of Silicone-based Electrically Conductive Adhesives and Conductive Backsheets for MWT Modules," *Energy Procedia,* vol. 55, pp. 444-450, 2014/01/01/ 2014, doi: https://doi.org/10.1016/j.egypro.2014.08.007.

[12] T. Meßmer, F. Demiralp, and A. Halm, "Low Cost Semi Automated Assembly Unit for Small Size Back Contact Modules and Low Cost Interconnection Approach," *Energy Procedia,* vol. 98, pp. 98-105, 2016/11/01/ 2016, doi: https://doi.org/10.1016/j.egypro.2016.10.085.

[13] I. J. Bennett, R. H. A. Janssen, F. van Duijnhoven, and J. Xu, "Development of conductive back-sheet for manufacture of PV modules with back-contact cells," *2018 IEEE 7th World Conference on Photovoltaic Energy Conversion (WCPEC) (A Joint Conference of 45th IEEE PVSC, 28th PVSEC & 34th EU PVSEC),* pp. 3623-3625, 2018.

[14] H. Schulte-Huxel, S. Blankemeyer, A. Merkle, V. Steckenreiter, S. Kajari-Schröder, and R. Brendel, "Interconnection of busbar-free back contacted solar cells by laser welding," *Progress in Photovoltaics: Research and Applications,* https://doi.org/10.1002/pip.2514 vol. 23, no. 8, pp. 1057-1065, 2015/08/01 2015, doi: https://doi.org/10.1002/pip.2514.

[15] H. Schulte-Huxel, S. Blankemeyer, V. Steckenreiter, S. Kajari-Schroeder, and R. Brendel, "Laser-welded Interconnection of Screen-printed Si Solar Cells," *Energy Procedia,* vol. 55, pp. 356-360, 2014/01/01/ 2014, doi: https://doi.org/10.1016/j.egypro.2014.08.102.

[16] J. Paschen, P. Baliozian, O. John, E. Lohmüller, T. Rößler, and J. Nekarda, "FoilMet®-Interconnect: Busbarless, electrically conductive adhesive-free, and solder-free aluminum interconnection for modules with shingled solar cells," *Progress in Photovoltaics: Research and Applications,* https://doi.org/10.1002/pip.3470 vol. 30, no. 8, pp. 889-898, 2022/08/01 2022, doi: https://doi.org/10.1002/pip.3470.

[17] K. Fisher, X. Meng, B. Hartweg, S. Mony, M. Bertoni, and Z. Holman, "Novel Foil Interconnects for Back-Contact Silicon Solar Cells," in *2019 IEEE 46th Photovoltaic Specialists Conference (PVSC)*, 16-21 June 2019 2019, pp. 0126-0130, doi: 10.1109/PVSC40753.2019.8980924.

[18] J. Wohlgemuth, "IEC 61215: What it is and isn't," presented at the 2012 PV Module Reliablity Workshop, February 29, 2012, 2012, NREL/PR-5200-54714.

[19] *Terrestrial photovoltaic (PV) modules - Design qualification and type approval - Part 2: Test procedures*, IEC, 2021.

[20] O. John *et al.*, "Laser Metal Bonding (LMB) - low impact joining of thin aluminum foil to silicon and silicon nitride surfaces," *Procedia CIRP,* vol. 94, pp. 863-868, 2020/01/01/ 2020, doi: https://doi.org/10.1016/j.procir.2020.09.109.
[21] "JMP Statistical Discovery LLC." https://www.jmp.com/en_us/home.html (accessed.
[22] H. Schulte-Huxel, R. Bock, S. Blankemeyer, A. Merkle, and R. Brendel, "Aluminum-based mechanical and electrical laser interconnection process for module integration of silicon solar cells," *IEEE Journal of Photovoltaics,* vol. 2, no. 1, pp. 16-21, 2012, doi: 10.1109/JPHOTOV.2011.2177072.
[23] J. Paschen, A. Nägele, O. John, G. Emanuel, and J. Nekarda, "FoilMet®-connect: Upgrading adhesion by the application of laser metal bonding," *AIP Conference Proceedings,* vol. 2709, no. 1, p. 020002, 2022/11/15 2022, doi: 10.1063/5.0126335.